Influence of Electrode Geometric Arrangement on the Operation of Narrow Circular Electrostatic Precipitator

A. Niewulis[1, 2], J. Podliński[1], A. Berendt[1], J. Mizeraczyk[1, 3]

[1] Centre for Plasma and Laser Engineering, The Szewalski Institute of Fluid Flow Machinery, Polish Academy of Sciences, Fiszera 14, 80-231 Gdańsk, Poland
[2] Mathematics Teaching and Distance Learning Centre, Gdańsk University of Technology, ul. Narutowicza 11/12, 80-233 Gdańsk, Poland
[3] Department of Marine Electronics, Gdynia Maritime University, Morska 81-87, 81-225 Gdynia, Poland
Email of corresponding author: jmiz@imp.gda.pl

Abstract—In this work the influence of electrode geometric arrangement on the operation of an circular electrostatic precipitator (ESP) was investigated using Particle Image Velocimetry (PIV) method. The ESP was a glass circular cylinder (29 mm in diameter, 300 mm long) equipped with a wire discharge electrode and circular-cylinder collecting electrode. The stainless-steel discharge wire electrode (0.23 mm in diameter, 100 mm long) was mounted either in the centre (concentric case) or off-centre of the cylinder (eccentric case), parallel to the cylinder axis. The circular-cylinder electrode was grounded. Positive voltage up to 10 kV was supplied to the wire-electrode through a 10 MΩ resistor. Air flow seeded with a cigarette smoke was blown axially along the ESP duct with an average velocity of 0.9 m/s. Also the case without forced axial flow was studied. The results showed that the eccentricity of the wire electrode with regard to the ESP axis is an important parameter influencing the operation of the circular ESP. Regardless of the discharge current intensity, a small shift of the wire electrode from the ESP axis (the eccentricity smaller than 8 %) did not change the discharge current intensity at constant operating voltage. However, when the eccentricity of the wire electrode exceeded 8 %, the discharge current intensity increased with increasing shift of the wire electrode from the ESP axis at constant operating voltage. But apart from that the discharge current flowing to that part of the collecting electrode which was nearer to the wire electrode was higher than that of the other part. The intensity of the discharge current to the closer part of collecting electrode increased with decreasing distance between the discharge electrode and the collecting electrode. The PIV measurements showed that eccentricity of the wire position influenced also the structure of the dust particle flow in the circular ESP. When the discharge wire was set almost ideally along the ESP cylinder axis, the dust particles moved radially towards the collecting circular-cylinder electrode. In contrast, an eccentricity in the wire position caused a severe disturbance in the radial movement of the particles, generating particle flow vortices. This can result in a lower collection efficiency of the dust particles in the ESP with eccentric wire electrode.

Keywords — narrow electrostatic precipitator, ESP, EHD flow, flow measurement, PIV

INTRODUCTION

Recently narrow electrostatic precipitators (ESPs) (having the cross section of several cm^2) have become a subject of interest because of their possible application in diesel engines for the exhausted particulate matter collection [1-9]. Narrow ESPs can also be used in self-pumped electrohydrodynamic (EHD) devices for air cleaning [10-14].

The precipitation of particles in the duct of an ESP depends on fluid flow parameters, dust-particle properties, electric field and space charge, and electrode geometry.

The coupling of the two-phase fluid flow fields, the electric field and the electric space charge field in the ESP generate the so-called EHD secondary flow in the ESP duct. Study of such a coupling of several fields in ESPs is a difficult task. Dozens of papers have been devoted to the investigations of the field coupling in ESPs and resulting flow patterns [e.g. 15-21]. The flow patterns in the ESP depend also on the electrode shape and electrode geometric arrangement. In our previous experimental studies of the narrow cylindrical ESP operation we found that the narrow cylindrical ESPs are particularly sensitive to the symmetry of wire electrode positioning in regard to the ESP cylinder. Our experimental observations were partly confirmed by a computational investigation of the airflow patterns induced in a circular cylindrical tube with the discharge wire electrode positioned either concentric or eccentric [22].

In this paper we present results of the investigations of influence of the electrode arrangement in a narrow circular ESP on its operation regarding the discharge current distribution on the collecting electrodes and the dust particle flow patterns.

EXPERIMENTAL PROCEDURE AND SETUP

The ESP used in the present work was a narrow cylindrical glass tube in which a wire discharge electrode and a circular-cylinder collecting electrode were mounted (Fig. 1). The stainless-steel discharge wire electrode (0.23 mm in diameter, 100 mm long) was mounted either in the centre (concentric configuration, Fig. 2a) or off-centre (eccentric configuration, Fig. 2b) of the circular-cylinder collecting electrode, parallel to the axis of the electrode. The eccentric configuration (Fig. 2b) was realized by parallel displacing the wire electrode from the collecting electrode axis toward the collecting electrode surface. The eccentricity (ε) of the wire electrode was changed from 4 % to 47 % (the eccentricity is defined as the ratio of the wire displacement from the cylinder axis to the cylinder radius). Two stainless-steel circular-cylinder collecting electrodes (25.5 mm in diameter, 200 mm long) were used in this experiment. The first was cut longitudinally, as shown in Figs. 1a and 2, the second - transversely (Fig. 1b). The first collecting electrode consisted of two circular half-cylinders: A and B (Figs. 1a and 2). The second collecting electrode was formed from two shorter circular-cylinders, each having a length of 100 mm (Fig. 1b).

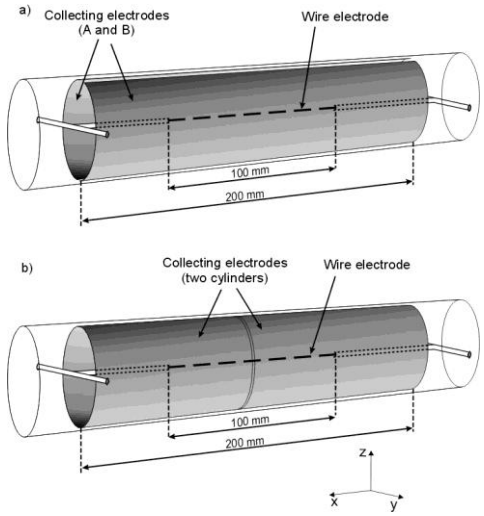

Fig. 1. Circular ESP with longitudinally (a) and transversely (b) cut collecting circular cylinder-electrodes.

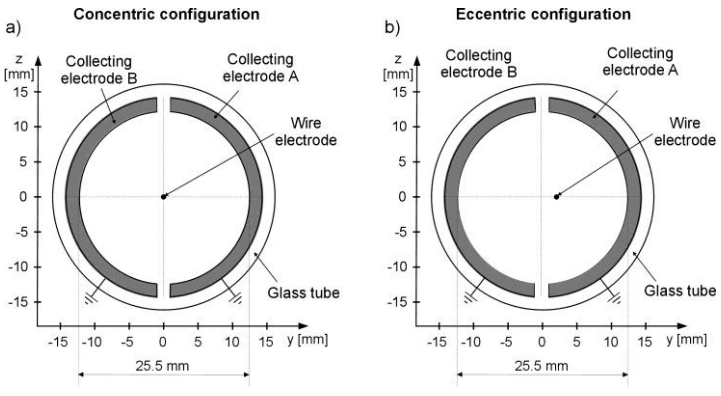

Fig. 2. Transverse cross section of the narrow circular ESP (with the longitudinal cut). a) Concentric configuration, b) Eccentric configuration.

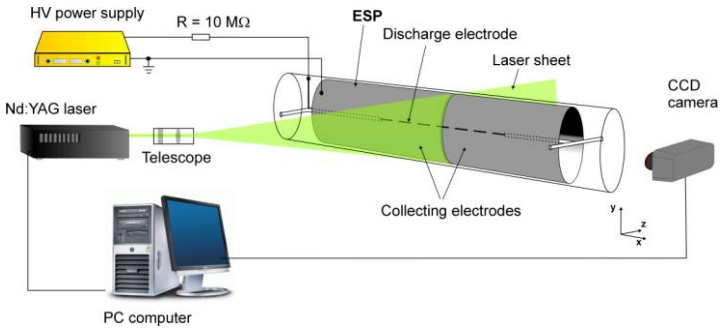

Fig. 3. The experimental setup for the measurement of EHD flow patterns in the transverse cross section of ESP using PIV.

The first ESP with two collecting half-cylinders A and B (Figs. 1a and 2) was used in the measurements of the total discharge current division to the electrodes A and B, when the wire electrode was displaced parallel to the ESP axis. A high-voltage DC power supplier model SL50PN300 (Spellman High Voltage Electronics Corporation) was used to run the discharge. Positive voltage up to 10 kV (always measured between the wire-electrode and the collecting electrode) was supplied to the wire-electrodes through a 10 MΩ resistor. The half-cylinders were grounded through two amperemeters Metex model M-4650CR. The discharge currents flowing to electrodes A and B were measured using these amperemeters.

The second ESP with two shorter collecting cylinders (Fig. 1b) was used for PIV measurements of the transverse flow patterns in the ESP. A short gap distance between both cylinders (2 mm) enabled introducing a laser plane beam (called the laser sheet) between the shorter cylinders, perpendicularly to the wire and the cylinders, whereby the PIV measuring was possible. The experimental apparatus for the measurement of flow patterns (Fig. 3) used in the present work consisted of the ESP with two shorter-cylinder collecting electrodes, high voltage supply and standard 2D PIV equipment [23].

PIV method enables determining the flow velocity vectors in a selected cross-section of the flow, called the observation plane. The observation plane is fixed in the flow by introducing into it a laser plane beam, called the laser sheet. If the laser sheet is assumed to be infinitely thin, a single CCD camera is used for monitoring the observation plane. This enables measuring two components of the velocity vectors which are parallel to the observation plane (the so-called 2D PIV case). The measurement of velocity vector field is based on the observation of the movement of flow seeding particles that cross the observation plane. The particle movement is determined by monitoring the laser sheet light scattered by the particles. The scattered laser light forms the flow image that is recorded by the CCD camera. From two successive images of the observation flow the velocity vector field of the seeding particles can be determined. When the seeding particles follow the gas flow, the seeding particle

velocity field is assumed to be mapping the gas flow velocity field. In the other case, PIV method delivers the seeding particle velocity field in the flow.

The velocity fields presented here describe two cases. The first concerns instantaneous velocity fields. The other is a result of averaging of 100 measurements, which means that in this case each velocity map is time-averaged. The time used for capturing 100 measurements was 33 s.

In most experiments presented here, air flow seeded with cigarette smoke particles was axially blown along the ESP duct with an average velocity of 0.9 m/s. However, also the case without any forced axial flow was studied.

RESULTS AND DISCUSIONS

A. Discharge current division

A.1 Without forced axial air flow

Here we present the case when there was no axial air flow forced in the ESP.

The time-averaged discharge current-voltage characteristics for two selected positions of wire electrode (in the centre of the ESP (concentric case) and at 0.5 mm from the axis of the ESP, i.e. for ε = 4%) are shown in Fig. 4.

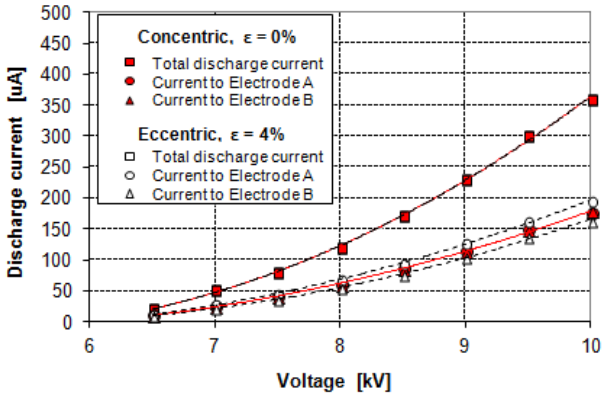

Fig. 4. Discharge current-voltage characteristics for two selected position of the wire electrode (concentric - ε = 0% and eccentric - ε = 4%).

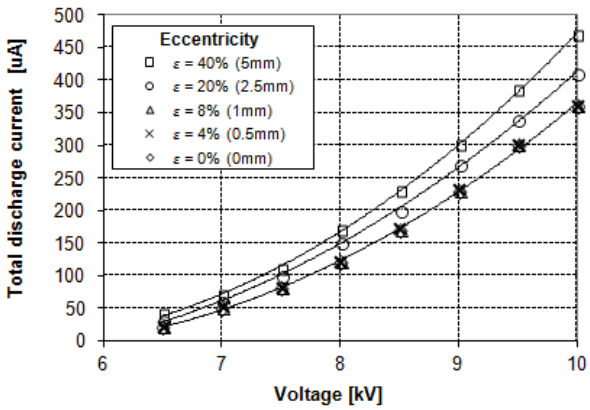

Fig. 5. Total discharge current (to electrode A and B) as a function of voltage for five eccentricities of the wire electrode.

It is seen in Fig. 4 that the total discharge currents (to the electrode A and B) were the same for the concentric (ε = 0 %) and eccentric (ε = 4 %) cases.

However, the eccentricity of the wire electrode affected the intensity of the individual discharge currents flowing to the each of separated half-cylinders (the current to the half-cylinder A and to the half-cylinder B). For the same voltage applied to the wire electrode the individual discharge current to the electrode A (that being nearer to the wire electrode) was higher than that to electrode B.

The total discharge current (to electrode A and B) as a function of applied voltage for five eccentricities of the wire electrode are shown in Fig. 5. It is seen from Fig. 5 that for the eccentricities of the wire electrode up to 8 % (i.e. the displacement of the wire electrode from the axis of the ESP up to 1 mm) the total discharge current remained constant. However, when the eccentricities was longer than 8 % the total discharge current increased with increasing value of the eccentricity. For example, for positive polarity voltage of 10 kV the total discharge current was about 27 % higher for the wire electrode placed 5 mm from the ESP axis (ε = 40 %) than that for concentric case (ε = 0).

The individual discharge currents to electrodes A and B as a function of voltage for five eccentricities of the wire electrode are shown in Fig. 6. As can be seen, the individual discharge current to the half-cylinder A (the nearer to the wire electrode) was higher than that to half-cylinder B. Furthermore, the individual discharge current to the half-cylinder A increased with decreasing distance between the discharge wire electrode and collecting electrode.

Fig. 7 shows the top view images of the corona discharge in the circular ESP with the wire electrode placed either ideally (ε = 0 %) along the ESP cylinder axis or 2.5 mm off the ESP axis (ε = 20 %). Usually the positive corona is manifested as a plasma uniformly distributed along the wire electrode. When the corona occurs in air, the homogeneous plasma shines blue.

As can be seen in Fig. 7a the corona discharge in the concentric-configuration ESP was uniformly distributed over the entire surface of the wire electrode. However, in the eccentric-configuration ESP the distribution of corona discharge was different. More discharge was located on this surface of the wire electrode that was closer to the collecting electrode (half-cylinder A), exhibiting stronger glow on that part of wire electrode (Fig. 7b). The brighter glow wire surface which is closer to electrode A is consistent with the higher individual current to electrode A.

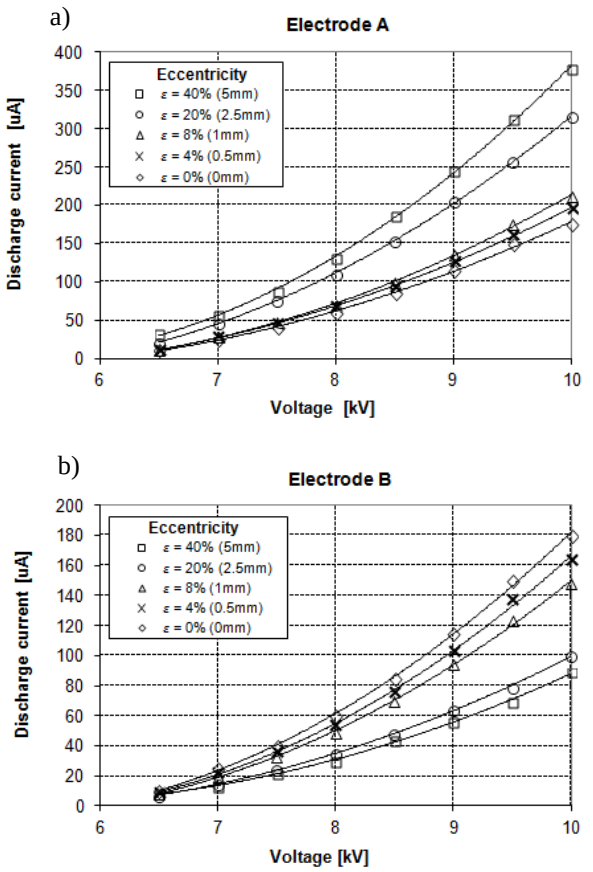

Fig. 6. Individual discharge currents to electrode A (a) and B (b) as a function of voltage for five eccentricities of the wire electrode.

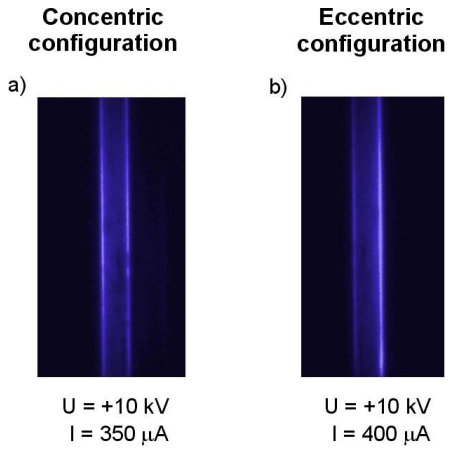

Fig. 7. Top view images of the corona discharge on the wire electrode in the circular ESP: a) Concentric configuration (ε = 0 %), b) Eccentric configuration (ε = 20 %).

A.2 With forced axial air flow

Here we present the results for the case when seeded or unseeded air was flowing with an average velocity of 0.9 m/s along the ESP. The results are compared with those obtained in the ESP with no axial flow (unseeded air).

Fig. 8 shows the total discharge current as a function of time in the circular ESP with the wire electrode placed ideally along the ESP cylinder axis (ε = 0). One can see that in the case with forced axial flow the total discharge current decreased of about 10 % in comparison with the case without forced axial flow.

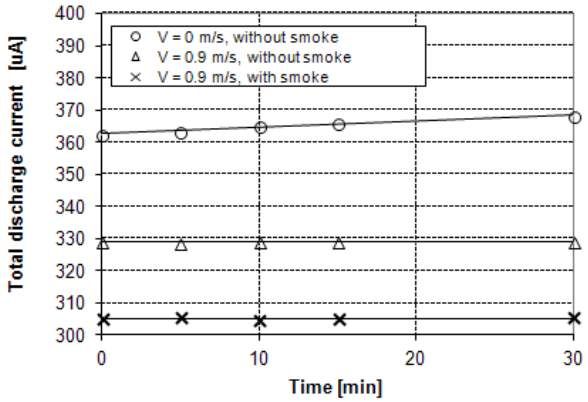

Fig. 8. Total discharge current as a function of time in the circular ESP with wire electrode placed along the ESP axis (ε = 0 %).

For the former case the total discharge current did not change in the time course of the measurement. However, without axial air flow the total discharge current increased by about 2 % in 30 minutes after the discharge onset. This could be caused by heating effects which must have occurred due to lack of the heat convection in the absence of axial air flow.

The result in Fig. 8 show that total discharge current intensity was depends on concentration of the seed particle concentration. The increase of the seed particles concentration in the flow resulted in a decrease of the total discharge current intensity. This is consisted with earlier results presented in [24].

B. Flow velocity field patterns

B.1 Without forced axial air flow

B.1.1 Concentric configuration

Before starting the measurements of velocity field patterns in the circular ESP for the case without forced axial flow, the ESP was filled with uniformly seeded air (the seed particles will be called by us the dust particles since they are collected by the ESP).

Results of the time evolution of particle flow patterns in the circular ESP with wire electrode placed in the ESP centre (ε = 0 %) without forced axial flow are shown in Fig. 9. The typical instantaneous records of the laser light scattered by the dust particles are presented in the left column, while the right column shows flow patterns (i.e. flow streamlines and velocity field), both in the transverse mid-plane (the y-z plane) of the ESP for different time elapses. The laser light scattered by the dust particles illustrates the presence or absence of the particles in a given volume. If the particles are present in the given volume, they scatter the laser light and camera (or an eye) records this volume as a bright area (green in this case, because the laser light is green). The volume with no dust particles is recorded as a black area (no scatter). The bright (green) and black areas show where the dust particles are present and where are absent, respectively.

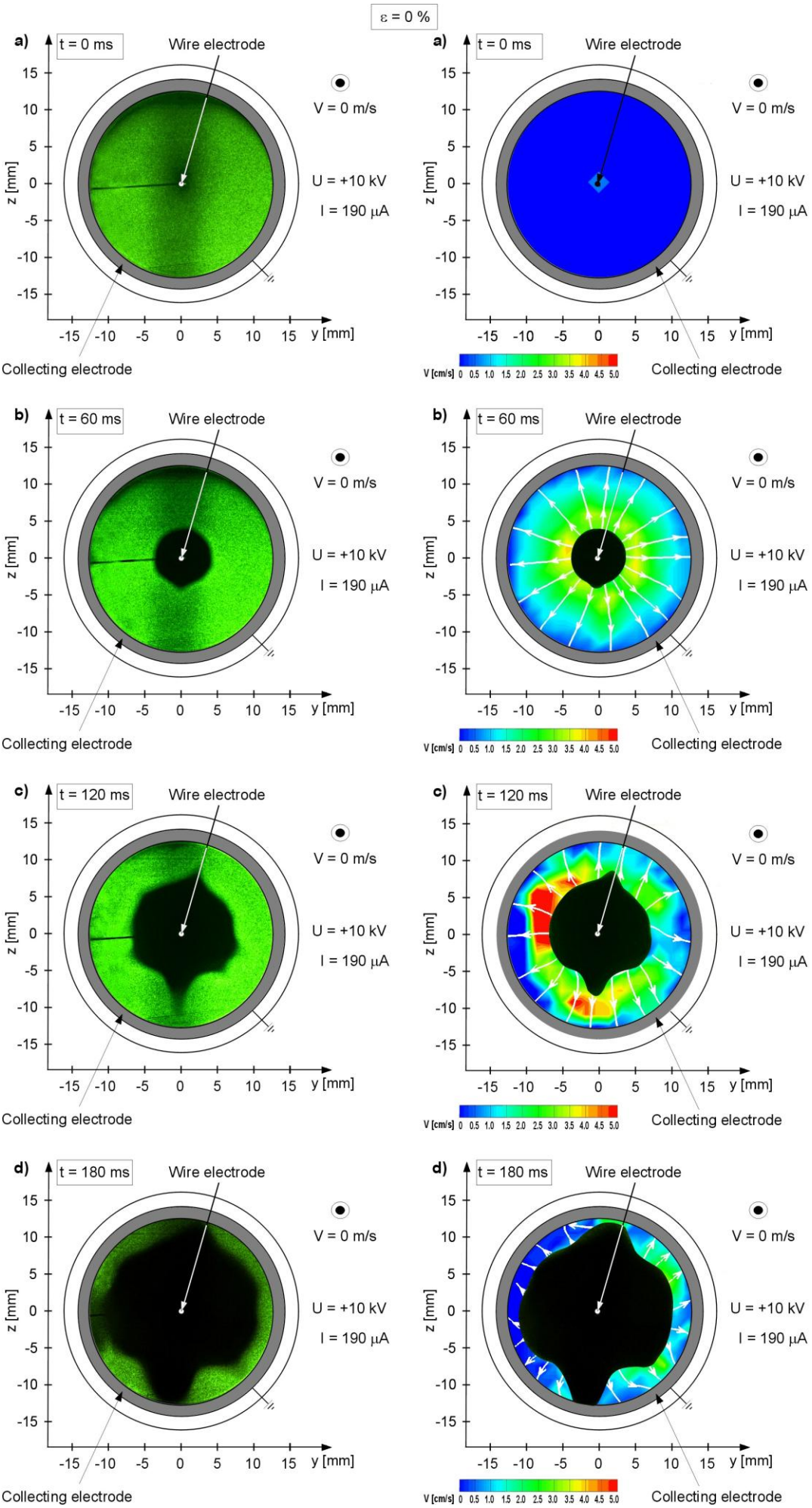

Fig. 9. Time evolution of the structures of the dust particle flow after applying high voltage in the concentric circular ESP (ε = 0 %) without forced axial flow (v = 0 m/s). Instantaneous recordings of the laser green light scattered by dust particles - left column. Instantaneous flow patterns (velocity field, velocity streamlines) - right column. Positive voltage of 10 kV. Average total discharge current 190 μA.

The particle flow patterns in the circular ESP measured without applied voltage (Fig. 9a, left and right columns) show that there was no movement of the dust particles in the y-z plane. In this case the dust particles are motionlessly suspended in the air. After applying the high voltage of 10 kV, particle flow patterns started to develop around the wire electrode. The dust particles are pushed from the wire electrode outwards by the electric force which is strongest around the wire electrode (Figs. 9b-d, left and right columns). The dark areas around the wire electrode, seen in Figs. 9b-d, are the areas from which the particles have been removed (the brightness of an area image is higher for higher dust particle concentration, dark areas show places with no dust particles). With elapsing time "the particle removal wave" moves farther outward, making the dark particle–free areas around the wire electrode larger. After a time of 240 ms almost all of the particles suspended between the wire and the collecting electrode were removed from this space and deposited on the collecting electrode surface.

Generally, in the circular ESP with wire electrode placed along the ESP axis (concentric case), the particles move radially from the ESP centre to the the collecting electrode (see the velocity field in Figs. 9b-d). It can be found from Figs. 9b-d that the particle migration velocity changed from 8 cm/s in the axial region of the ESP to 0 cm/s near the collecting electrode.

B.1.2 Eccentric configuration

Results of the time evolution of the particle flow patterns in the circular ESP for two selected eccentricity of the wire electrode ($\varepsilon = 20$ %, corresponding to a distance of 2.5 mm from the ESP axis and $\varepsilon = 47$ %, i.e. 6 mm from the ESP axis) without forced axial flow are shown in Figs. 10-11, respectively.

Figs. 10-11 show, similarly as in the case of the concentric configuration (Fig. 9), typical instantaneous records of the laser light scattered by the dust particles (left column), and the flow patterns (i.e. flow streamlines and a velocity field, right column) in the transverse mid-plane (the y-z plane) of the ESP for different time elapses.

In both cases of the ESP with eccentric configuration ($\varepsilon = 20$ % and $\varepsilon = 47$ %) the dust particles were motionlessly suspended in the air before the high voltage was applied to the wire electrode. After applying the high voltage of 10 kV the transverse particle flow started to develop.

When the eccentricity $\varepsilon = 20$ %, at a time of 60 ms after applying the voltage the removal wave of the dust particles was circular (dark circular area, Fig. 10b) and had developed at a rate of 0.7 cm/s. With elapsing time the removal wave (dark area) of the dust particles move towards the right side of the collecting electrode (the side being nearer to the wire electrode). The flow streamlines in the Fig. 10c (right column) illustrate the motion of the dust particles in the form of two regular spiral vortices. At 120 ms after applying the voltage the migration velocity ranged from 0.7 m/s in the discharge region to below 0.01 m/s near the collecting electrode. Starting from about 180 ms after applying the voltage (Figs. 10d-f), the transverse dust particle transport became chaotic. This resulted in irregular and turbulent flow patterns of the dust particles. Despite of the flow irregularity the migration velocity of some particles reached values up to 1.5 m/s. With elapsing time the density number of dust particles in the ESP continuously decreased. Finally, after 480 ms all of the particles were deposited on the collecting electrode.

In the circular ESP with eccentricity of wire electrode $\varepsilon = 47$ % (Fig. 11) the flow patterns was similar as in the circular ESP with eccentricity of wire electrode $\varepsilon = 20$ %, however the migration velocities of the dust particles were higher. Moreover, the pair of spiral vortices occurred earlier (60 ms after applying the voltage) and the dust particles were confined in the space between the wire and the collecting electrode longer (even at 1.3 s after applying the voltage).

The flow patterns described above are consistent with that predicted theoretically in [22].

B.2 With forced axial air flow

Results of the 2D PIV measurements for three selected position of wire electrode (in the centre of the ESP, i.e. for $\varepsilon = 0$ %; for 2.5 mm from the axis of the ESP, i.e. for $\varepsilon = 20$ %; and for 6 mm from the axis of the ESP, i.e. for $\varepsilon = 47$ %) are shown in Figs. 12-14, respectively. They show averaged records of the laser light scattered by the dust particles and averaged flow patterns (i.e. averaged flow streamlines and flow velocity field) in the transverse mid-plane of the ESP when the air flowed along the ESP with a velocity of 0.9 m/s (forced axial air flow case).

The transverse particle flow patterns in the circular ESP (concentric and eccentric configurations) measured without applied voltage (not presented here) showed a slight movement of the dust particles in the y-z plane, i.e. transversally to the axial air flow. This was caused by the axial air flow. However, the y- and z-velocity components were very low (below 0.01 m/s). In this case the submicron particles of the seed (called by us the dust particles) followed the axial air flow, and had the x-velocity component almost equal to the axial air flow velocity [20].

After applying the high voltage to the wire electrode (Figs. 12-14), the EHD forces generated by the corona discharge induced a transverse flow in the y-z plane, i.e. transversely to the flow duct.

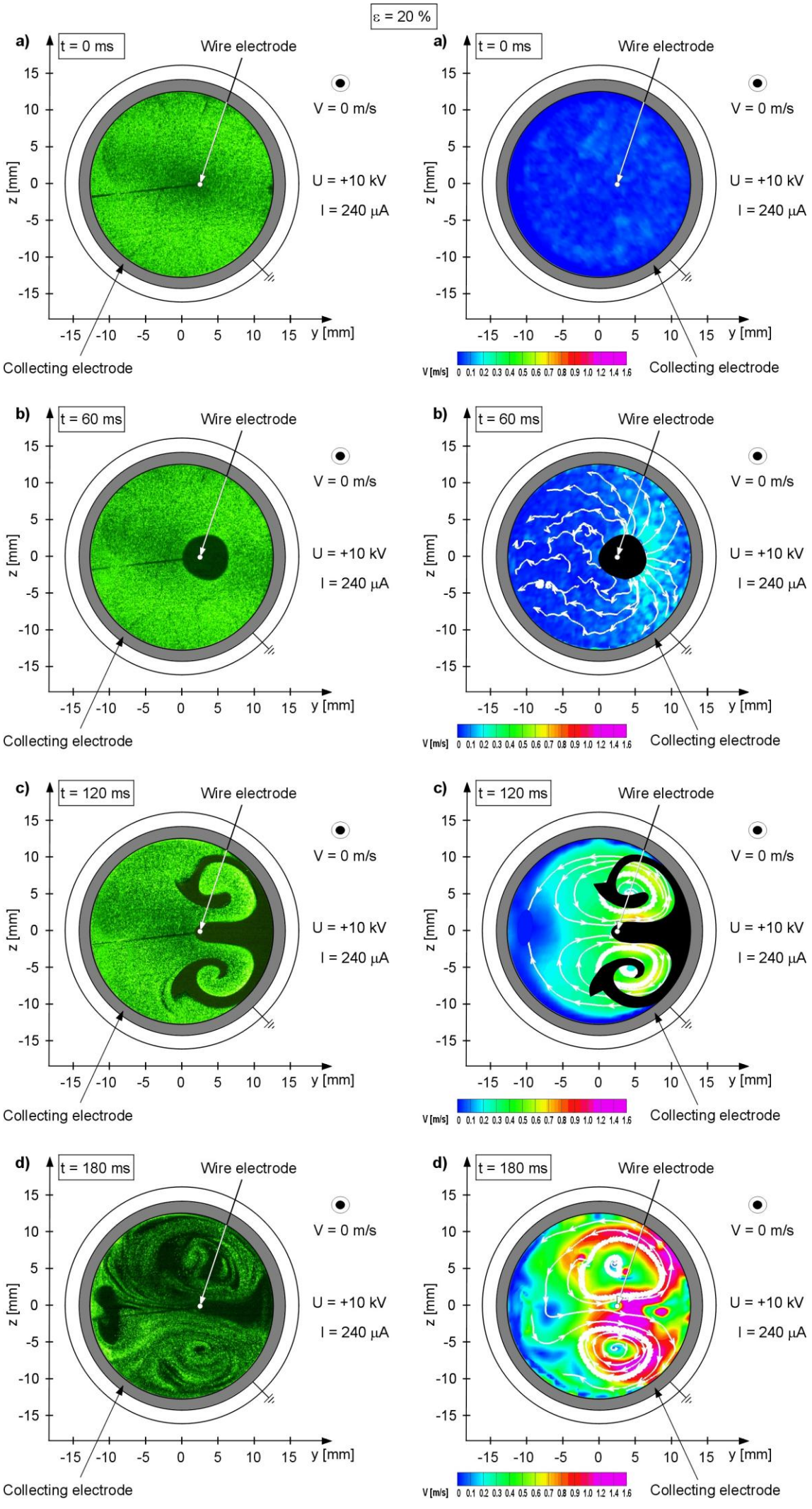
ε = 20 %
a)
t = 0 ms
Wire electrode
V = 0 m/s
U = +10 kV
I = 240 μA
Collecting electrode
z [mm]
y [mm]
V [m/s] 0 0.1 0.2 0.3 0.4 0.5 0.6 0.7 0.8 0.9 1.0 1.2 1.4 1.6
b)
t = 60 ms
c)
t = 120 ms
d)
t = 180 ms

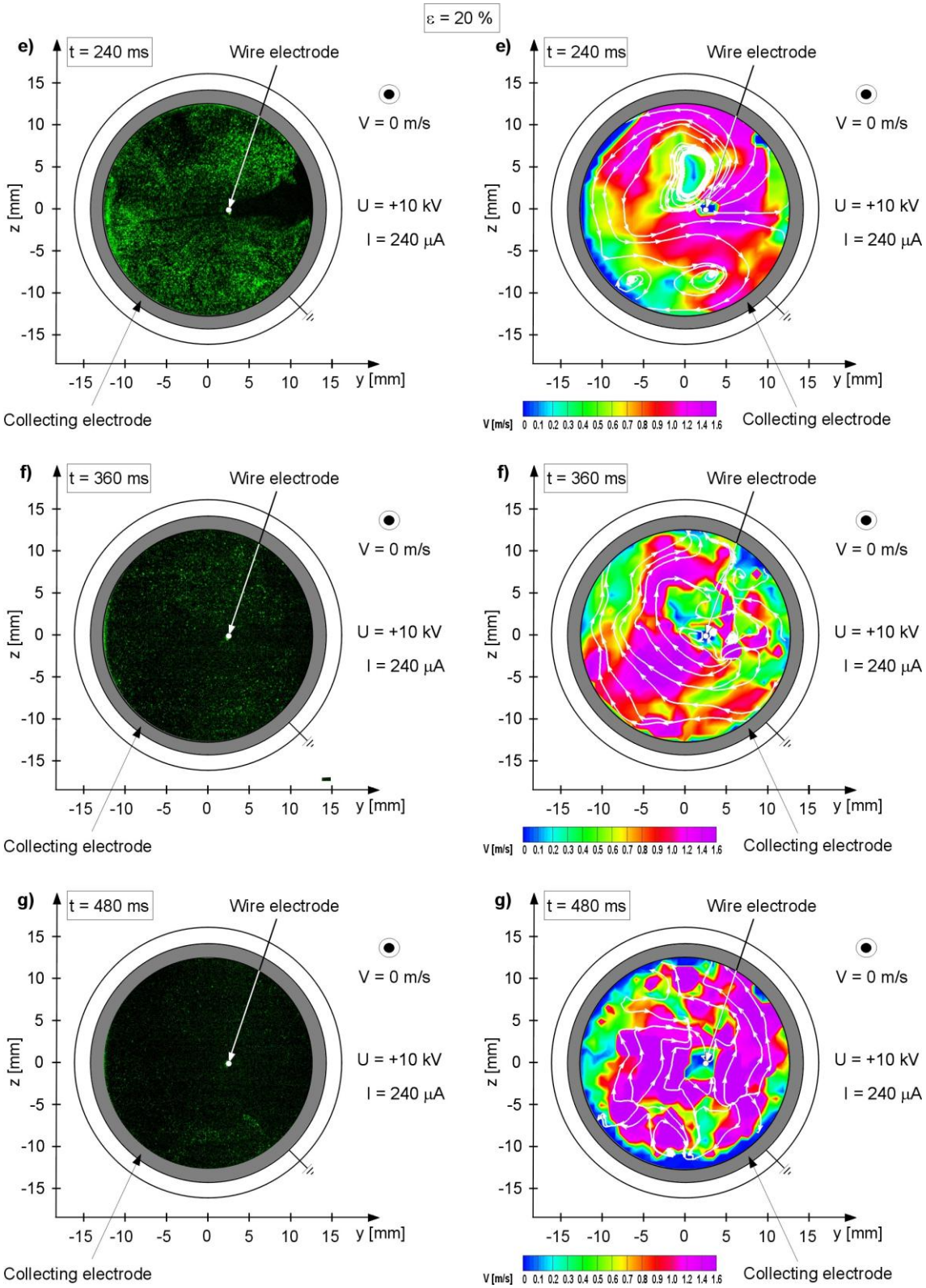

Fig. 10. Time evolution of the structures of the dust particle flow after applying high voltage in the eccentric circular ESP (ε = 20 %) without forced axial flow (v = 0 m/s). Instantaneous recordings of the laser green light scattered by dust particles - left column. Instantaneous flow patterns (velocity field, velocity streamlines) - right column. Positive voltage of 10 kV. Average total discharge current 240 μA.

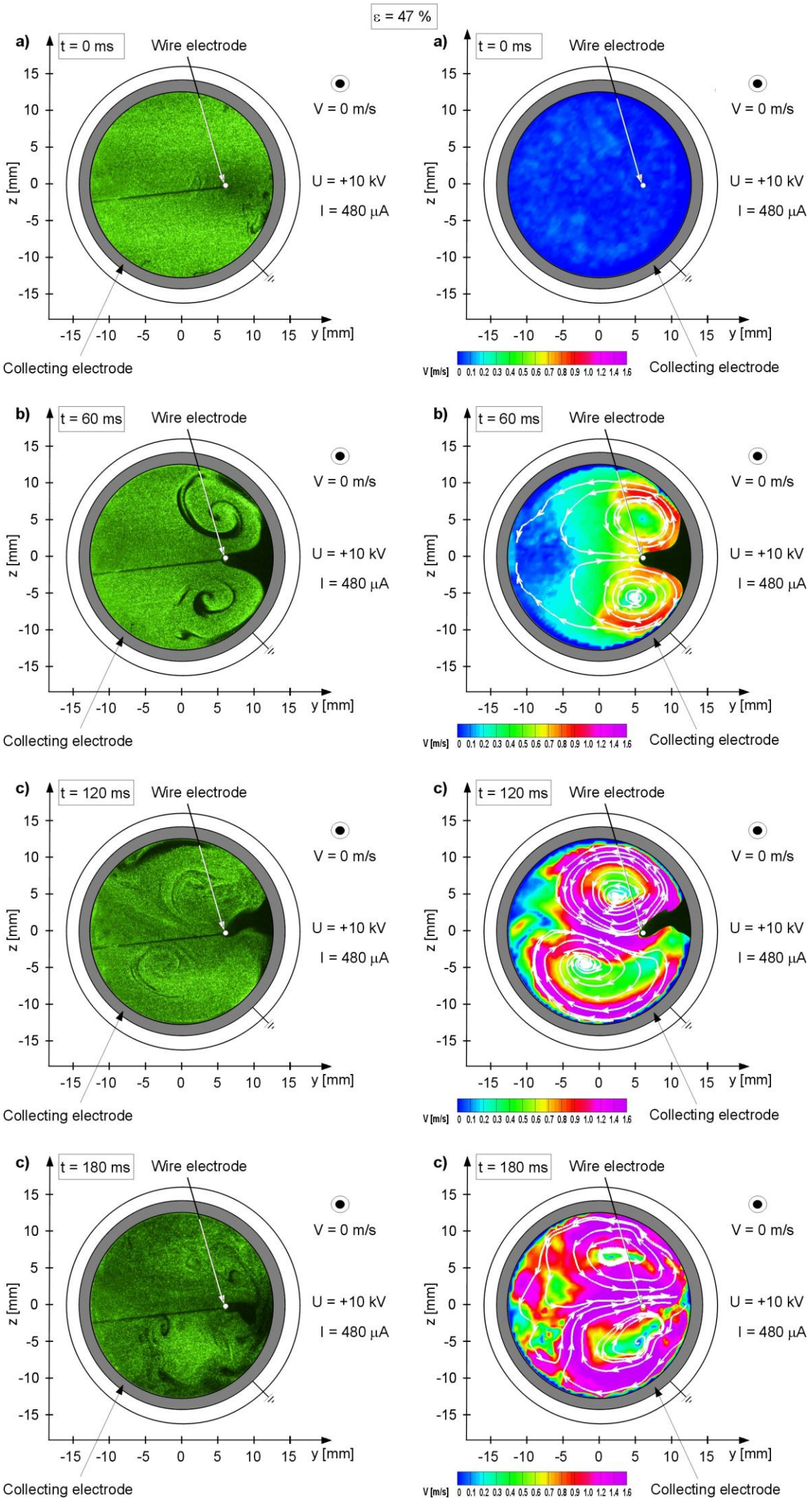
ε = 47 %
a)
t = 0 ms
Wire electrode
V = 0 m/s
U = +10 kV
I = 480 μA
Collecting electrode
b)
t = 60 ms
c)
t = 120 ms
t = 180 ms
z [mm]
y [mm]
V [m/s] 0 0.1 0.2 0.3 0.4 0.5 0.6 0.7 0.8 0.9 1.0 1.2 1.4 1.6

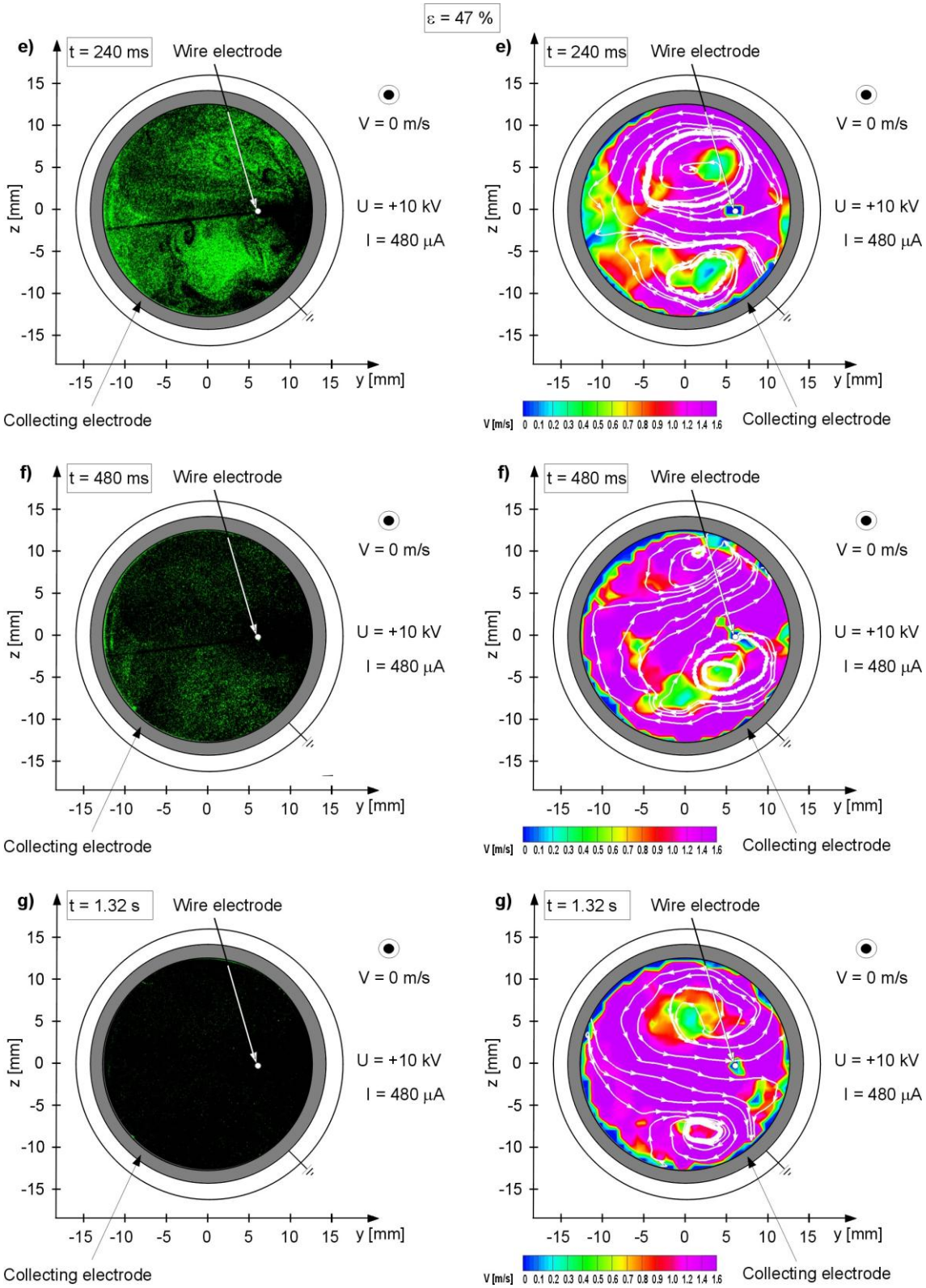

Fig. 11. Time evolution of the structures of the seed particle flow after applying high voltage in the eccentric circular ESP (ε = 47 %) without forced axial flow (v = 0 m/s). Instantaneous recordings of the laser green light scattered by dust particles - left column. Instantaneous flow patterns (velocity field, velocity streamlines) - right column. Positive voltage of 10 kV. Average total discharge current 480 μA.

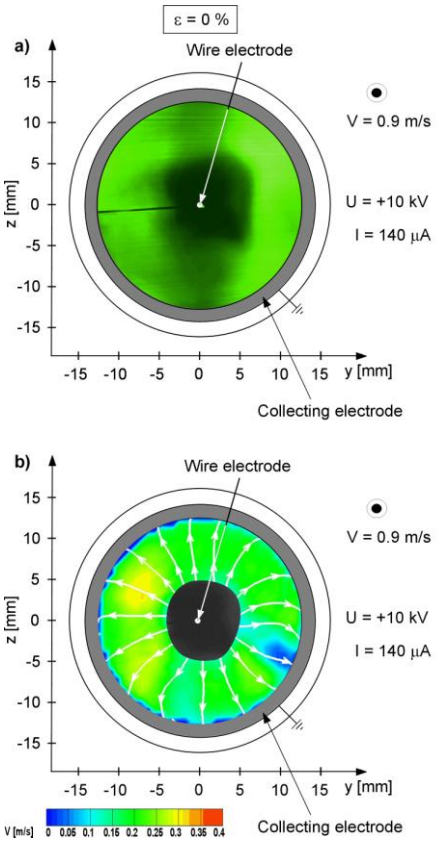

Fig. 12. Averaged recording of the laser green light scattered by dust particles (a) and flow patterns (velocity field, velocity streamlines) (b) in the concentric circular ESP (ε = 0 %) with forced axial flow (v = 0.9 m/s). Positive voltage of 10 kV. Average total discharge current 140 μA. ⦿ - shows the direction of the forced axial flow

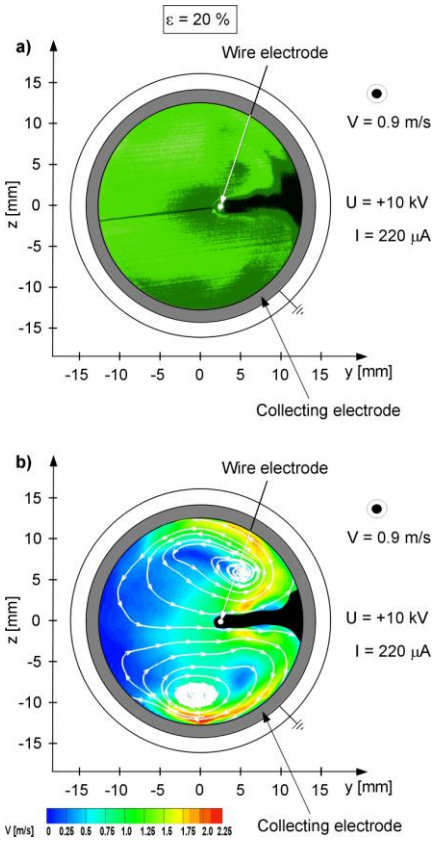

Fig. 13. Averaged recording of the laser green light scattered by dust particles (a) and flow patterns (velocity field, velocity streamlines) (b) in the eccentric circular ESP (ε = 20 %) with forced axial flow (v = 0.9 m/s). Positive voltage of 10 kV. Average total discharge current 220 μA. ⦿ - shows the direction of the forced axial flow

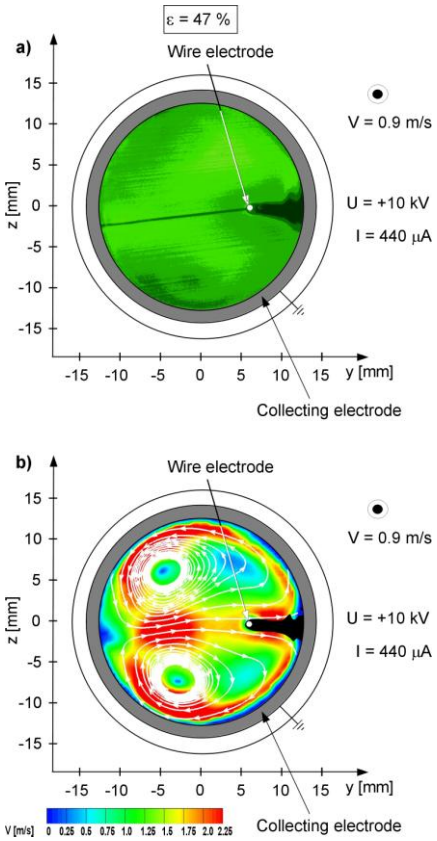

Fig. 14. Averaged recording of the laser green light scattered by dust particles (a) and flow patterns (velocity field, velocity streamlines) (b) in the eccentric circular ESP (ε = 47 %) with forced axial flow (v = 0.9 m/s). Positive voltage of 10 kV. Average total discharge current 440 μA. ⦿ - shows the direction of the forced axial flow

B.2.1 Concentric configuration

In the circular ESP with concentric wire electrode the particle flow towards the collecting electrode was very regular (Fig. 12).

The strong electric field and the space charge around the stressed wire electrode caused fast removal of the dust particle from the zone near the wire electrode. The dark circular zone around the wire electrode seen in Fig. 12a is the area from which the particles have already been removed.

In Fig. 12 similar effect as in the circular ESP with wire electrode placed in the ESP centre (ε = 0 %) without forced axial flow (Fig. 9) can be observed: the particle trajectories moved radially from the ESP centre (i.e. from the discharge wire-electrode) towards the collecting electrode. As can be seen from Fig. 12, the transverse flow confirms the pattern of the particle flow presented in Fig. 9b. However, the particle velocities for the concentric circular ESP with forced axial flow are higher than those for the concentric case without forced axial flow.

B.2.2 Eccentric configuration

The eccentric configuration of the circular ESP disturbed the transverse symmetry of the flow typical of the concentric configuration.

It is seen from Figs. 13-14 that due to the EHD force the particles flow from the discharge wire electrode towards the right side of the collecting electrode (the side being nearer to the wire electrode). Then, near the cylinder electrode the particles disperse forming two flows which move along the cylinder surface in the opposite directions. These two particle flows meet on the other side of the cylinder and are forced to move to the cylinder centre and then towards the wire electrode. As seen from Fig. 14 the charged particles moving towards the wire electrode are slowed down by the electric field formed by it. As a result, two vortices, rotating in opposite directions, are formed in the y–z plane. Although our measurements were two-dimensional the analysis of the obtained results showed that the observed vortices exhibit three-dimensional character, having the form of a spiral vortex moving along the ESP. The size and shape of the vortex depends on the eccentricity of the wire position.

In the circular ESP with wire electrode placed 2.5 mm from the ESP axis (ε = 20 %, Fig. 13) the vortices are formed in the region adjacent to the wire electrode. In the circular ESP with wire electrode placed 6 mm from the ESP axis (ε = 47 %, Fig. 14) the vortices are shifted to the left, farther from the wire electrode.

Moreover, Figs. 13-14 show, that the dust particles velocity increased with increasing shift of the wire electrode from the ESP axis at constant operating voltage. In the first case (ε = 20 %) the dust particles rotate with the velocity up to 1.75 m/s, whereas in the second case (ε = 47 %) the dust particles rotate with the velocity up to 2.5 m/s. These spiral vortices may decrease the particles collection efficiency.

SUMMARY AND CONCLUSIONS

Our experiment confirmed that the eccentricity of the wire electrode is an important parameter influencing the operation of the circular ESP. Regardless of the total discharge current, a very small shift of the wire electrode from the ESP axis (the eccentricity smaller than 8 %) did not change significantly the discharge current at constant voltage. However, when the eccentricity of the wire electrode was higher than 8 %, the total discharge current increased with increasing shift of the wire electrode from the ESP axis. In the ESP with separated collecting electrodes the individual discharge current was higher for collecting electrode being nearer to the wire electrode and increased with decreasing distance between the discharge electrode and collecting electrode.

The PIV measurements showed that an eccentricity of the wire position influenced the structure of the transverse dust particle flow in the circular ESP. When the discharge wire was set almost ideally along the ESP cylinder axis, the dust particles moved radially towards the collecting circular cylinder electrode. However, an eccentricity in the wire position caused a severe disturbance of the radial movement of the particles, generating flow vortices.

An experiment is planned to find if an eccentricity of the wire electrode affects the electrostatic precipitator collection efficiency.

ACKNOWLEDGMENT

This work was supported by the Ministry of Science and Higher Education (grant PB 281/T02/2010/70, grant PB 7475/B/T02/2011/40).

REFERENCES

[1] D.P. Thimsen, K.J. Baumgard, T.J. Kotz, "The Performance of an Electrostatic Agglomerator as a Diesel Soot Emission Control Device", *SAE Paper* 900330, pp. 173-182, 1990.

[2] D.B. Kittelson, J. Reinersen, J. Michalski "Further Studies of Electrostatic Collection and Agglomeration of Diesel Particles", *SAE Paper* 910329, 145-163, 1991.

[3] M. Farzaneh, A.K. Marceu, P. Lachance, "Electrostatic Capture and Agglomeration of Particles Emitted by Diesel Engines", *IEEE*, pp. 1534-1537, 1994.

[4] C. Wadenpohl, F. Loeffler, "Electrostatic agglomeration and centrifugal separation of diesel soot particles", *Chemical engineering and processing* 33 (5), pp. 371-377, 1994.

[5] T. Ciach, T. R. Sosnowski, "Removal of soot particles from diesel exhaust", *Journal of Aerosol Science*, Volume 27 (1), pp. S705-S706, 1996.

[6] A. Zukeran, Y. Ikeda, Y. Ehara, M. Matsuyama, T. Ito, T. Takahashi, H. Kawakami, T. Takamatsu, "Two-Stage-Type Electrostatic Precipitator Re-Entrainment Phenomena Under Diesel Flue Gases", *IEEE Transactions On Industry Applications*, vol. 35, No. 2, 1999.

[7] Ph. Saiyasitpanich, T. C. Keenera, S. J.Khangb, M. Lua, "Removal of diesel particulate matter (DPM) in a tubular wet electrostatic precipitator", *J. Electrostatics*, vol. 65, pp. 618–624, 2007.

[8] R. Boichot, A. Bernis, E. Gonze, "Agglomeration of diesel particles by an electrostatic agglomerator under positive DC voltage: Experimental study", *J. Electrostatics*, vol. 66, pp. 235–245, 2008.

[9] T. Yamamoto, T. Mimura, N. Otsuka, Y. Ito, Y. Ehara, A. Zukeran, "Diesel PM Collection for Marine and Automobile Emissions Using EHD Electrostatic Precipitators" *Industry Applications, IEEE Transactions on*, 46, pp.1606 – 1612, 2010.

[10] L. Leger, E. Moreau, F. Artana and G. Touchard, "Influence of a DC corona discharge on the airflow along an inclined flat plate", *J. Electrostatics*, vol. 51–52, pp. 300–306, 2001.

[11] H. Yanada, S. Hakama, T. Miyashita and N. Zhang, "An investigation of an ion drag pump using a needle–mesh electrode configuration", *The Proc. Instn. Mech. Engrs., Part C: Journal of Mechanical Engineering Science*, vol. 216, no. 3 pp. 325-334, 2002.

[12] L. Zhao and K. Adamiak, "EHD flow in air produced by electric corona discharge in pin–plate configuration", *J. Electrostatics*, vol. 63, pp. 337–350, 2005.

[13] H. Tsubone , J. Ueno, B. Komeili, S. Minami, G.D. Harvel, K. Urashima, C.Y. Ching and J.S. Chang, "Flow Characteristics of DC Wire-non-parallel Plate Electrohydrodynamic Gas Pump", *J. Electrostatics*, vol. 66, pp. 151-121, 2008.

[14] A. Katatani, A. Mizuno "Generation of Ionic Wind by Using Parallel Located Flat Plates", *J. Inst. Electrostat. Jpn*., vol. 34, no. 4, pp. 187-192, 2010.

[15] J. S. Chang, P. A. Lawless, and T. Yamamoto, "Corona discharge processes", *IEEE Trans. Plasma Sci.*, vol. 19, no. 6, pp.1152 -1167, 1991.

[16] R. J. Peterson, J. H. Davidson "Modification of Gas Flow by Charged Particles *Proc. IEEE Ind. App. Soc. Ann. Meeting* (Denver), p. 1513, 1994.

[17] J. Mizeraczyk, J. Podliński, M. Kocik, R. Barbucha, J.S. Chang, A. Mizuno, "Experimental Results on Electrohydrodynamic Flow in Electrostatic Precipitators", 4th Asia-Pacific Int. Symp. on the Basic and Application of Plasma Technology, Cebu Workshop, Cebu, Philippines, 2005, pp. 29-33.

[18] J. Podliński, J. Dekowski, J. Mizeraczyk, D. Brocilo, J.S. Chang, "Electrohydrodynamic Gas Flow in a Positive Polarity Wire-Plate Electrostatic Precipitator and the

Related Dust Particle Collection Efficiency", *J. Electrostatics, vol.* 64, pp. 259-262, 2006.

[19] J.S. Chang, J. Ueno, H. Tsubone, G.D. Harvel, S. Minami and K. Urashima, "Electrohydrodynamically induced flow direction in a wire-non-parallel plate type electrode corona discharge", *J. Phys. D; Appl. Phys*., vol. 40, pp. 5109-5111, 2007.

[20] J. Podliński, M. Kocik, R. Barbucha, A. Niewulis, J. Mizeraczyk, A. Mizuno, 3D PIV Measurements of the EHD Flow Patterns in a Narrow Electrostatic Precipitator with Wire-Plate or Wire-Flocking Electrodes, *Czechoslovak Journal of Physic*, 56, Suppl. B, 1009-1016, 2006.

[21] J. Podliński, A. Niewulis, J. Mizeraczyk, "Electrohydrodynamic flow in a wire-plate non-thermal plasma reactor measured by 3D PIV method", *European Physical Journal D*, 54, 153–158, 2009.

[22] R.B. Lakeh, M. Molki, "Patterns of Airflow in Circular Tubes Caused by a Corona Jet With Concentric and Eccentric Wire Electrodes", J. Fluids Engineering, vol.132, pp. 1-10, 2010.J. Westerweel, Fundamentals of Digital PIV, *Meas. Sci. Tech.* vol. 8, 1379-1392, 1997.

[23] M. Raffel, Ch.E. Willert, J. Kompenhans, *Particle Image Velocimetry, A practical guide*, Springer-Verlag Berlin Heidelberg, 2007.

[24] J. Podliński, A. Niewulis, J. Mizeraczyk, P. Atten, „ESP performance for various dust densities" *J. Electrostatics*, vol. 66, pp. 246-253, 2008.